Available online at www.sciencedirect.com
ScienceDirect
Journal of the European Ceramic Society 29 (2009) 3053–3061
www.elsevier.com/locate/jeurceramsoc

Inelastic deformation under indentation and scratch loads in a ZrB_2–SiC composite

Dipankar Ghosh [a], Ghatu Subhash [a,*], Gerald R. Bourne [b]

[a] *Department of Mechanical and Aerospace Engineering, University of Florida, Gainesville, FL 32611, USA*
[b] *Major Analytical Instrument Center, Department of Materials Science and Engineering, University of Florida, Gainesville, FL 32611, USA*

Received 27 January 2009; received in revised form 3 April 2009; accepted 15 April 2009
Available online 17 May 2009

Abstract

Inelastic deformation features induced in an ultra-high temperature ceramic composite, ZrB_2–SiC, due to static indentation (rate of deformation of the order of $10^{-5}\ s^{-1}$), dynamic indentation (rate of deformation of the order of $10^3\ s^{-1}$), and high-velocity scratch (500 mm/s) experiments are presented. It was found that this ceramic composite has up to 30% higher dynamic hardness compared to static hardness. Dynamic indentations resulted in extensive transgranular microcracking within the indented regions compared to static indentations. In addition, significant plastic deformation features in terms of slip-line formation were observed within statically and dynamically indented regions. The high-velocity scratch studies revealed extensive transgranular microcracking perpendicular to the scratch direction and slip-lines in and around the scratch path. Preliminary transmission electron microscopy (TEM) observations from regions of slip-lines surrounding the scratch grooves revealed dislocation activity in the composite.

Keywords: Electron microscopy; Hardness; Borides; Silicon carbide; Plasticity

1. Introduction

Ultra-high temperature materials (UHTMs) are central to the development of structural components (e.g., external heat shields, nose cones, leading edges) for future high performance aircrafts, hypersonic vehicles, kinetic energy interceptors and reusable space planes owing to their light weight, high melting temperature, strength retention at elevated temperatures, and superior oxidation resistance.[1,2] These UHTMs are intended to operate in severe reactive environments with temperatures well above the melting points of traditional materials. A promising candidate in this class of materials is zirconium diboride–silicon carbide (ZrB_2–SiC) composite which has low density ($5.84\ g/cm^3$), high melting temperature (>3000 °C) and improved oxidation resistance above 1500 °C.[1,2] While in service (e.g., during take off, landing, or reentry in to atmosphere) the aforementioned structural components are prone to impact by meteorites and atmospheric debris particles at very high velocities. Evolution of damage and fundamental inelastic deformation mechanisms should be fully understood to evaluate the suitability of ZrB_2–SiC for the above applications. Although these composites are intended to be used at high temperatures, investigation of quasistatic and dynamic responses at room temperature constitutes the first step towards a better understanding of their inelastic behavior in service.

Indentation and scratch testing methods have been popularly used on numerous engineering materials to reveal fundamental deformation mechanisms that are operative during wear, abrasion, impact and machining processes.[3–7] Typically, indentation and scratch studies are conducted at extremely low velocities, resulting in deformation strain rate on the order of $0.001\ s^{-1}$. During several engineering applications such as high-speed grinding, projectile impact, atmospheric particle impact on the protective tiles of an aerospace vehicle, material deforms within a few hundreds of microseconds or milliseconds resulting in strain rate of deformation about $10^3\ s^{-1}$ or higher. Thus, the traditional static indentations and the low-velocity scratches do not fully capture the inherent material strain rate effects that are operative under service conditions. For example, many materials exhibit increased yield strength.[8–10] fracture strength[10,11] and fracture toughness[12,13] under dynamic loads.

In this manuscript we will focus on deformation mechanisms evolved during static and dynamic indentations, and during high-velocity scratch processes in ZrB_2–SiC composite. Recently, the

* Corresponding author. Tel.: +1 352 392 7005; fax: +1 352 392 7303.
E-mail address: subhash@ufl.edu (G. Subhash).

0955-2219/$ – see front matter © 2009 Elsevier Ltd. All rights reserved.
doi:10.1016/j.jeurceramsoc.2009.04.014

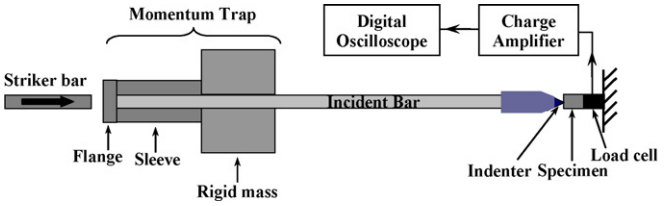

Fig. 1. Schematic of the experimental setup for dynamic indentation hardness measurements.

authors have reported some preliminary results of indentation study in this composite.[14] In the current manuscript new results on static and dynamic indentation behavior of the ZrB_2–SiC composite are presented. The authors have also previously conducted detailed experimental and analytical investigations of low-load and low-velocity scratch behavior of ZrB_2–SiC composite,[15] and these results will briefly be presented here to compare with the high-velocity scratch studies.

2. Experimental

2.1. Material and specimen preparation

In the current work, a ZrB_2–5 wt% SiC composite tile of dimensions 75 mm × 52 mm × 8 mm processed using plasma pressure compaction method.[15] The composite had a 96% theoretical density (5.84 g/cm^3). The average grain sizes of the ZrB_2 phase and SiC phase, estimated from fragmented surfaces of the composite, were 5 μm and less than 1 μm, respectively. For indentation and scratch experiments, specimens of dimensions 6 mm × 3 mm × 3 mm were cut from the composite tile and one of the rectangular surfaces was ground and polished using standard metallographic techniques.

2.2. Static and dynamic indentations experiments

Static indentations (15 s duration) were conducted on the polished surfaces of the composite at loads of 300, 500, 1000 and 2000 g using a conventional Vickers microhardness tester. Dynamic hardness measurements of 100 μs duration were conducted in the similar load range employing a dynamic Vickers indentation hardness tester.[13] This method, developed by Subhash, is based on elastic stress wave propagation phenomena in a slender rod.[13] The hardness tester assembly consists of a slender rod, a momentum trap (MT), a striker bar, an indenter housing, and a high frequency (200 kHz) Kistler load cell as shown in Fig. 1. The slender rod (also called 'incident bar') houses a Vickers indenter at one end and a momentum trap (MT) assembly at the other end. The MT assembly consists of a flange, a sleeve and a rigid mass. The specimen is sandwiched between the indenter and the load cell which is mounted on a rigid base.[13] Upon impact of the indenter on to the MT-end of the incident bar, the generated stress waves will ensure that a single compressive stress pulse reaches the indenter-end. This pulse causes the indenter move forward and creates indentation on the specimen. The rest of the stress wave causes the indenter to retract. The dynamic hardness is calculated based on the measured indentation diagonal size on the specimen and the load measured by the load cell. This method has been successfully utilized to determine the dynamic Vickers indentation hardness of several metallic and ceramic materials,[13] and negative strain rate sensitivity of hardness in bulk metallic glasses as well as variation in shear band spacing.[17]

2.3. Low- and high-velocity scratch experiments

Previously, low-velocity (5×10^{-3} mm/s) constant load scratch experiments of 200 μm scratch length were conducted in a MTS nanoindenter® XPS system using a Berkovich nanoindenter.[15] Scratch loads were varied in the range of 50–250 mN. The high-velocity (∼500 mm/s) scratch experiments were conducted in a custom-built instrumented scratch tester.[16] The specimen was held on top of a high frequency (200 kHz) load cell which was housed in a rigid steel block. The load cell measures the normal force (thrust) during the scratch process. The indenter tool (a diamond conical indenter with 90° included angle) was held in a pendulum holder that was supported by two high-precision ball-bearing bushings housed in a rigid steel frame. A pneumatically driven piston was used to swing the pendulum and cause the diamond tip to transverse a path of circular arc, and create a scratch of variable depth on the specimen surface. Total scratch length and maximum depth-of-cut of each scratch can be varied by changing the length of the tool in the pendulum holder.

2.4. Characterization

A field emission gun (FEG) scanning electron microscope (SEM) (JEOL 6335F) was used to investigate the indentation- and scratch-induced deformation and fracture characteristics in the ZrB_2–SiC composite. For identification of deformation features at a finer scale, transmission electron microscopy (TEM) was conducted. A site specific cross-sectional FIB (FEI Strata DB235) technique[19] was employed to prepare TEM specimens from the scratch groves. The FIB technique employs a focused galium ion (Ga^+) beam to prepare a thin TEM specimen of less than 200 nm thickness (of approximate dimensions 15 μm × 6 μm) from the target material through sputtering action. Here a "lift-out" technique[18] was used where an electron transparent thin specimen is cut-out from the bulk material and analyzed directly in TEM. First the area of interest (i.e., the region within a scratch groove containing large number of slip-lines) was protected from any potential damage from the Ga^+ ion beam by depositing a thin layer of platinum (Pt). Then, progressively deeper trenches were cut on either side to form a thin specimen as shown in Fig. 2 illustrating a FIB-cut transverse cross-sectional sample within a constant load scratch groove of 250 mN. The specimen was then cut through the depth on two ends (where the specimen is attached to the bulk of the material) so as to relax the residual stress (without cracking) which had developed as a result of elastic–plastic deformation during the scratch process. The beam current was then reduced and milling was performed on both sides of the sample until thinned down to thickness of about 200 nm. The specimen was

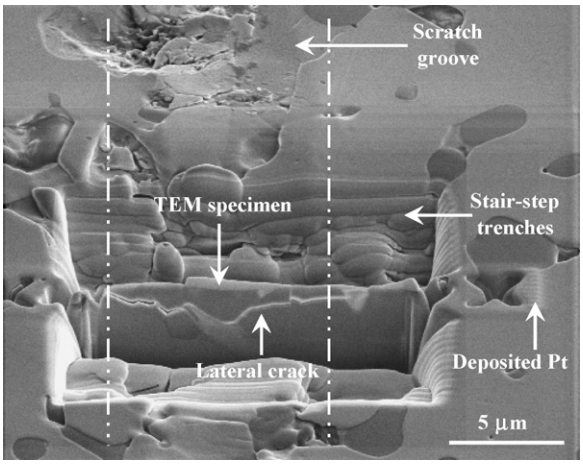

Fig. 2. FIB-cut TEM specimen within a constant load (250 mN) scratch groove.

set free from the scratch groove and analyzed in a TEM (JEOL 200CX).

3. Results

3.1. Static and dynamic indentations

A comparison of the measured static hardness and dynamic hardness vs. indentation load is shown in Fig. 3(a). The static hardness values were obtained at selected fixed loads where as the dynamic hardness values were measured over a range of loads by changing the velocity of the striker. The load dependency of static hardness, known as indentation size effect (ISE), can be seen in Fig. 3(a), i.e., a decrease in hardness value with increasing load. The dynamic hardness values, measured in the load range of 300–2000 g, were consistently greater than the static values at similar load levels. These measurements revealed large scatter, which is common for brittle materials under dynamic loads.[13] In contrast to static hardness, dynamic hardness measurements did not reveal any ISE. It is possible that the considerable amount of scatter in the dynamic hardness values probably masked load dependency of dynamic hardness. The trend in dynamic hardness response for ZrB_2–SiC composite is typical of many strain rate sensitive ceramic materials where hardness[13] and fracture strength[10,11,13] increase with strain rate. This behavior is expected due to the increased resistance of material against penetration under dynamic loads as will be discussed later in Section 4.

To evaluate the trend in these measurements, the dynamic hardness values were normalized by the static hardness values at the same load level and plotted with respect to the strain rate ($\dot{\varepsilon}$) in Fig. 3(b). Recall that the strain rate is not constant during an indentation test, rather varies temporally and spatially within the influence zone of indentation. At the beginning, the material directly beneath the indenter-tip experiences a higher strain rate due to higher indenter velocity as the sharp tip penetrates into a small region. With increasing depth of penetration, the contact area of the indenter increases (and hence the resistance to penetration) which results in a reduced indenter velocity resulting in a decrease in the strain rate. Therefore, the strain rate

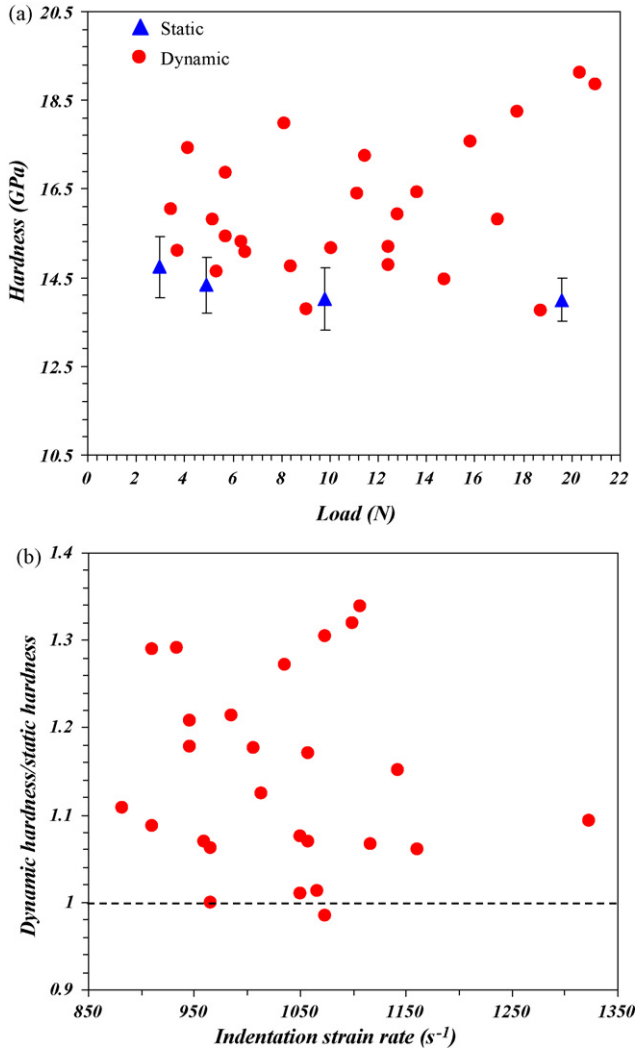

Fig. 3. (a) Comparison of static and dynamic hardness vs. indentation load and (b) plot of normalized dynamic hardness vs. strain rate.

is non-uniform throughout the influence region of indentation. Subhash[13] defined an average strain rate as the ratio of average indenter velocity and average indentation diagonal length. Since in the current work, average indenter velocity was not measured, it was approximated in the following way: from the measured diagonal lengths of dynamic indents and using the known geometry of the Vickers indenter, the depth of penetration was calculated (elastic recovery was neglected). A ratio of calculated penetration depth and total loading duration (known from load cell measurements) yielded the average indenter velocity. It can be seen from Fig. 3(b) that the calculated strain rate values fall in the range of 850–1350 s^{-1} which is consistent with the previously reported values on other structural ceramics.[13] To calculate static hardness values at the measured dynamic loads, a trend-line was fit through the static hardness values in the plot shown in Fig. 3(a). Then a ratio of dynamic hardness to static hardness at similar load level was calculated and plotted with respect to the strain rate of dynamic indentation experiments. Fig. 3(b) clearly revealed that most of the normalized dynamic hardness values were above unity indicating the increase in hard-

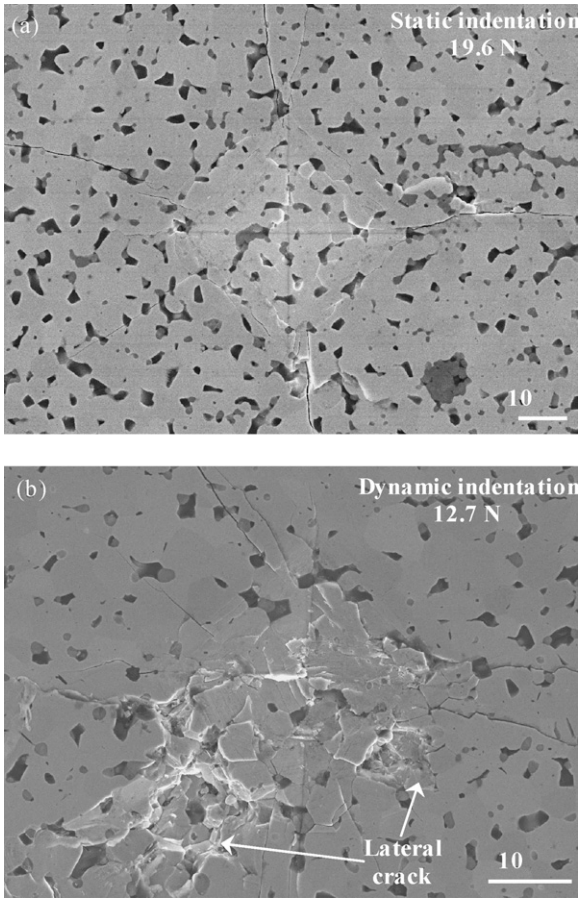

Fig. 4. SEM micrographs of (a) static and (b) dynamic indentations on the ZrB_2–SiC composite revealing greater brittle fracture under dynamic loading at lower load compared to static load.

ness under dynamic loading. The dynamic hardness value can be as high as 1.3 times the static value at any given load.

Fig. 4 shows typical static and dynamic indentations on the polished surfaces of the ZrB_2–SiC composite. From microstructural investigations, it was observed that macrocracking from the corners and sides of the indentation was limited when the load was 300 g. As the load increased above 300 g, cracks emanated from the corners and sides of the imprints. The intensity of cracking increased with indentation load. Interestingly, most of the cracks which emanated from the sides of indentation imprints were originated from the SiC phase. Microstructural investigations within the statically indented regions revealed that radial microcracks emanated from the ZrB_2 and SiC interfaces and propagated within the ZrB_2 matrix as shown in Fig. 5. Similar feature was also observed for dynamic indentations. However, the dynamic indentations resulted in extensive transgranular microcracking within the matrix phase inside the indented regions as shown in Fig. 6. Such a feature was not seen under static loads. Material removal by lateral crack formation was frequently observed under dynamic loading (Fig. 4(b)). Another interesting feature of indentations was the formation of slip-lines within the ZrB_2–SiC composite. Fig. 7 reveals static and dynamic indentation-induced slip-lines formed within the indented regions. Slip-line formation was also observed in

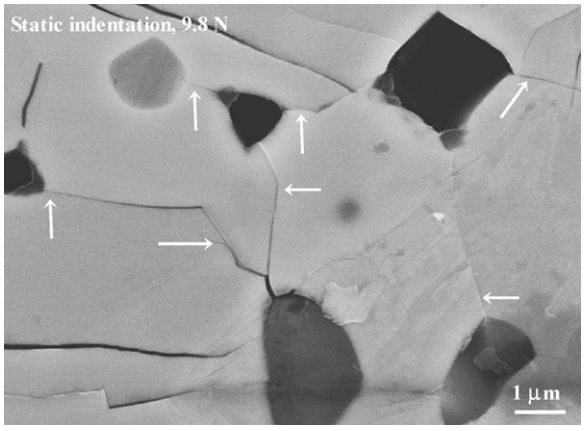

Fig. 5. Radial microcracks (indicated by small white arrows) originating from the interphases of ZrB_2 and SiC within a statically indented region.

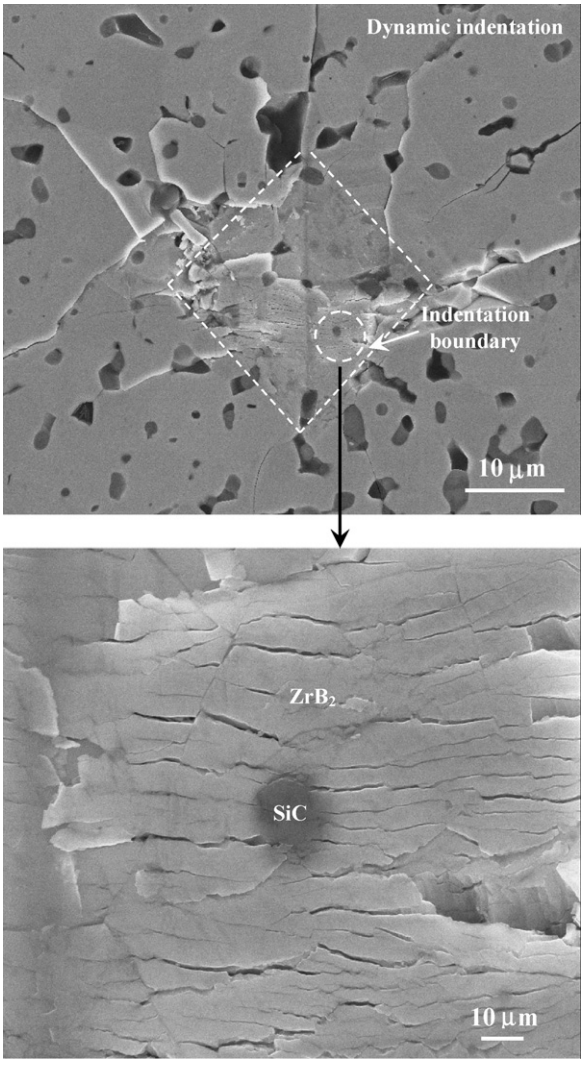

Fig. 6. Transgranular microcracking within the ZrB_2 matrix inside the dynamically indented region.

the regions slightly outside of the static and dynamic indents. These slip-lines were limited only to the ZrB_2 phase. Occasionally, transgranular microcracks were observed within these slip-band regions (see Fig. 7(b)). It can be observed that the slip-line patterns were similar across any given microcrack but their continuity was disturbed by transgranular microcracks, see Fig. 7(b). This observation indicated that slip-lines were formed first followed by the microcracking. The origin of transgranular microcracks within the ZrB_2 phase and the slip bands as well as microcracks at the ZrB_2–SiC interfaces will be discussed in more detail in section 4. As can be seen in these figures, no crack pattern was observed along the indentation, and therefore, it was not possible to calculate fracture toughness of the composite from indentation studies.

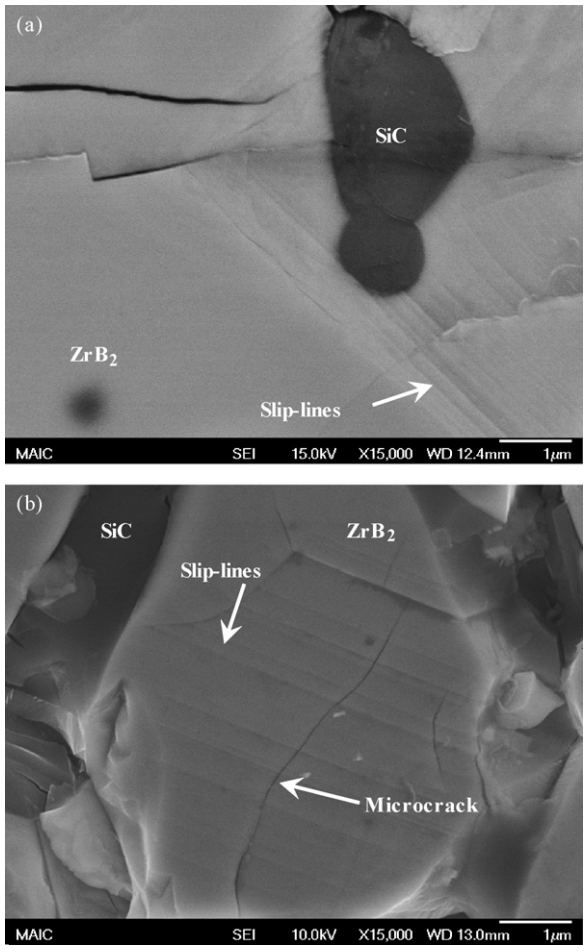

Fig. 7. Slip-line formation within the ZrB_2 phase in the ZrB_2–SiC composite due to (a) static and (b) dynamic indentations.

3.2. Low- and high-velocity scratches

Microscopic investigations of the constant load scratch grooves revealed that at low loads (<100 mN) smooth plastically deformed grooves with limited microscopic damage features were noted.[15] With increasing load, damage features became more prominent. High-resolution microscopy revealed mainly two inelastic deformation mechanisms within the scratch grooves: formation of multiple sets of slip-lines randomly oriented with respect to the scratch direction at all load levels and transgranular microcracks orthogonal to the scratch direction at higher scratch loads. Fig. 8(a) shows a residual scratch path at a constant load of 250 mN where as Fig. 8(b) reveals microscopic inelastic deformation features along the groove such as slip-lines and transgranular microcracks orthogonal to the scratch direction. At this load level, only limited lateral cracking was observed and material removal from the grooves occurred through transgranular fracture.

Fig. 9(a)–(c) reveal a high-velocity scratch path, formation of transgranular microcracks orthogonal to the scratch direction and the corresponding normal force vs. scratch length profile,

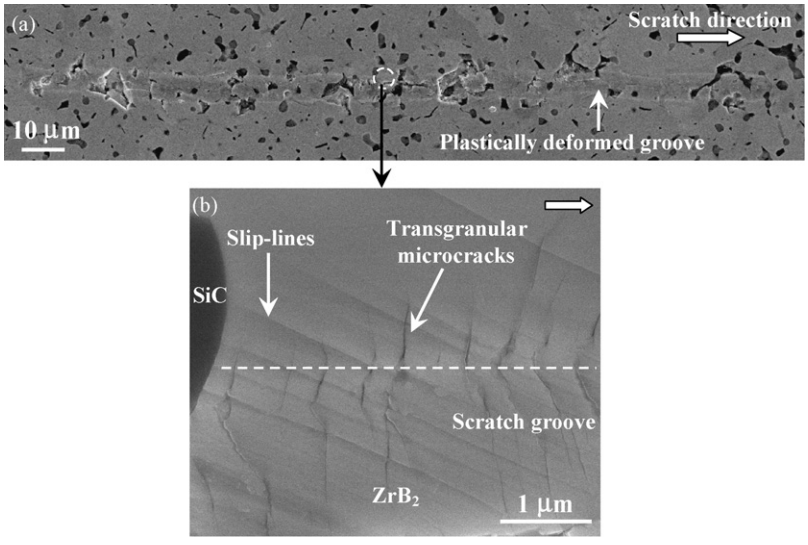

Fig. 8. (a) A constant load scratch path at 250 mN and (b) a higher magnification image of the region shown in (a) revealing slip-lines and microcracks within and outside of the scratch groove (the thick arrows indicate the scratch direction).

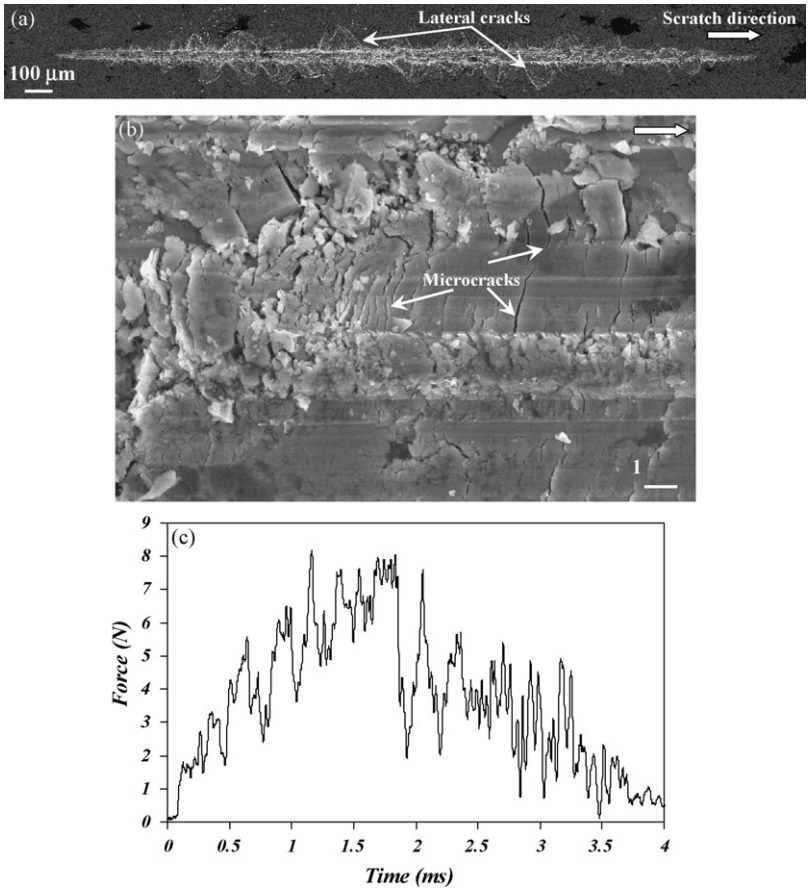

Fig. 9. (a) A high-velocity scratch groove, (b) high magnification images of extensive transgranular microcracks orthogonal to the scratch direction and (c) normal force vs. scratch length profile.

respectively. At the beginning of the scratch path, the load is small and hence the depth of the scratch groove is small which resulted in a smooth plastically deformed groove without any significant brittle damage. As the load increased, severe macroscopic brittle fracture features such as extended lateral cracking and material removal occurred in the middle of the scratch groove where the load was maximum. A closer view of the scratch groove revealed orthogonal transgranular microcracking and flattened debris, see Fig. 9(b). In high-velocity and high-load scratch experiments, the intensity of microcracking was significantly higher compared to previous scratch studies. Microstructural analysis of the regions containing lateral cracks also revealed the predominance of transgranular fracture in the composite. Similar to the indentation experiments, microplasticity in terms of slip-line formation was also observed in these high-velocity scratch grooves within the ZrB_2 phase. However, a majority of the regions containing slip-lines were probably removed due to extensive lateral cracking and the associated material removal. Thus, these studies revealed that during high-velocity scratch process, extensive transgranular microcracking and lateral cracking caused significant damage and material removal in the composite. The force profile (Fig. 9(c)) reveals that the load is minimum at the beginning and reaches maximum at the center of the scratches, and then again falls down to zero towards the exit end. Similarly, the scratch width is also minimum at both ends and maximum in the middle. The fluctuations in the force vs. distance profile are attributed to the brittle cracking and the associated material removal during the scratch process.

3.3. TEM investigations

The above indentation and scratch studies revealed that ZrB_2–SiC composite can exhibit considerable ductility in the form of slip-line formation within ZrB_2 matrix. Except a recent study on low-load scratch studies in this composite by the authors,[15] this mode of plastic deformation has not been reported in any polycrystalline UHTC in literature. However, in 1971, Haggerty and Lee[19] reported similar slip-line patterns in a single crystal ZrB_2 subjected to room temperature microindentation and high temperature compression tests. They identified dislocation motion and the associated slip systems through TEM studies. In the current investigation, TEM studies were initiated to identify the deformation-induced defect structure. The region of slip-line patterns in the indentation experiments were small and contained significant amount of cracking, and thus TEM specimens could not be prepared from indented regions. As mentioned before, high-velocity scratch grooves were heavily cracked followed by extensive lateral cracking in the surrounding areas. On the other hand, previously conducted low-load

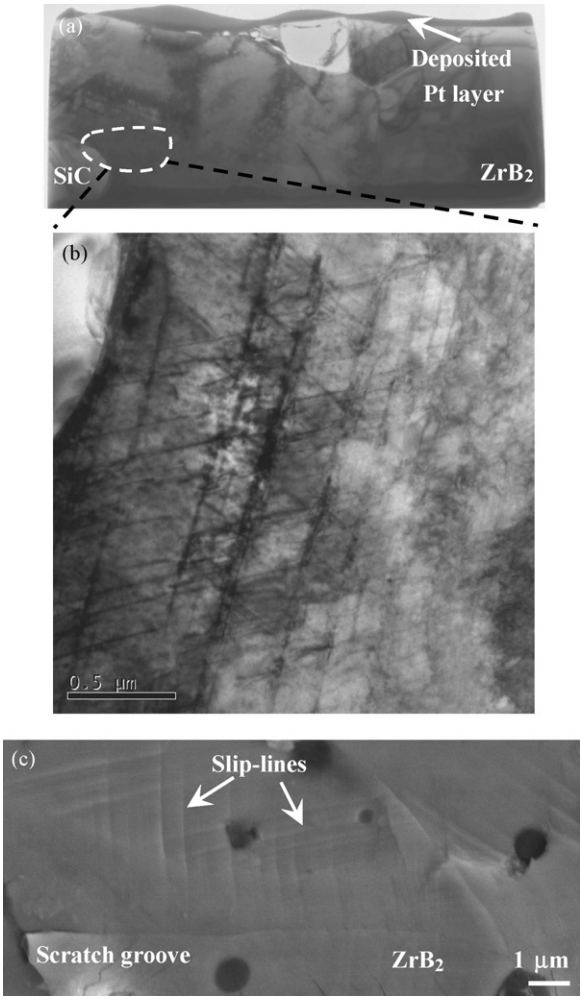

Fig. 10. (a) Bright-field image of a TEM specimen and (b) a higher magnification image of the region shown in (a) revealing activation of multiple slip systems. (c) A SEM micrograph of a constant load (250 mN) low-velocity scratch groove revealing multiple sets of slip-lines intersecting with each other within a single ZrB_2 grain.

scratch grooves were mostly crack free (see Fig. 8) and contained large areas of slip-lines. Therefore, these low-load scratch grooves were chosen for TEM specimen preparation. Here some preliminary results are presented. More detailed investigations are in progress and will be available at a later time. A low magnification bright-field image of the TEM specimen is shown in Fig. 10(a) where as Fig. 10(b) presents a high magnification bright-field TEM image of a selected area from Fig. 10(a) revealing highly deformed region beneath the scratch groove. The image shows at least three different sets of dislocations in different orientations, suggesting the possibility of multiple slip system activation within the ZrB_2 phase as a result of the scratch process. This dislocation activity is assumed to have manifested macroscopically in terms of multiple sets of slip-lines intersecting with each other with in a single ZrB_2 grain as observed in Fig. 10(c). Thus, these preliminary TEM studies confirmed that dislocations were indeed activated in ZrB_2 under indentation and scratch loads, and resulted in the observed multiple slip-line patterns within the deformed regions. In-depth analysis of identification of active slip systems is under progress and will be reported elsewhere.

4. Discussions

The above static and dynamic indentations and high-velocity scratch studies revealed several inelastic deformation mechanisms in the ZrB_2–SiC composite. The evolved features such as transgranular microcracking, lateral cracking, and slip-line formation were limited only to the ZrB_2 matrix. In indentation studies, dynamic loading (or higher rate of deformation) resulted in considerable increase in the hardness compared to the static hardness, see Fig. 3. This observed increases in the composite could be a combined effect of strain rate sensitivities of the matrix (ZrB_2) and the SiC phases. However, dynamic mechanical response of pure ZrB_2 is not readily available in the open literature. SiC is known to exhibit increased hardness and fracture strength under high strain rate loading.[20] SiC also has high modulus and strength compared to ZrB_2, but as the volume fraction of ZrB_2 phase was significantly larger than the SiC content, it is reasonable to infer that a major contribution to observed increase in dynamic hardness of the composite arose from the ZrB_2 phase.

Although macrocracks were observed to emanate from the corners and the edges of imprints in both types of indentations (Fig. 4), extensive grain level microcracking appeared only in dynamic indentations, see Fig. 6. This microcracking feature is typical of ceramics when subjected to high-velocity impact[21–23] and high strain rate compressive loading.[24–26] Recently, Subhash et al. [14] presented a comprehensive review of dynamic indentation- and high-velocity impact-induced damage in ceramics, and found similarities in the damage patterns. More specifically, the dynamic indentation-induced cracking patterns were compared to those induced due to ball impact results reported by Normandia[22] and Iyer.[23] In high-velocity tungsten carbide sphere impact experiments on SiC plates, Iyer[23] correlated the observed damage features in various regions of the damaged specimen to the macroscopic triaxial stress field induced in the corresponding regions. In Iyer's work, the region directly beneath the impactor where a distributed three-dimensional network of grain boundary microcracks was observed is relevant to the current research.[23] In this region, a triaxial compressive stress state exists. Development of grain level microcracks was due to 'wing crack' growth from preexisting flaws in a ceramic subjected to compressive loads.[24–26] Under quasistatic loading such microcrack network was not observed. This result is explained on the basis of differences in damage growth characteristics under static and dynamic loads in ceramics.[9,24] During quasistatic loading only one single crack, most favorably oriented to the applied stress state, is activated. Under rapidly applied dynamic load, the inertia associated with the crack tip opening delays the crack growth but the applied stress rises rapidly to activate multiple cracks resulting in multiple crack growth and extensive microcracking. Thus it was inferred that the observed severe transgranular microcracks in the composite due to dynamic indentations originated due to high strain rate loading from the preexisting flaws and, there-

fore, dynamic indentation resulted in additional fracture within the ZrB_2–SiC composite which was not so prominent in the static indentation.

Microcracks observed within the slip-band regions may have originated as a result of severe plastic deformation within the indentation and scratch regions. Intensity of microcracks across and along the slip-lines was more prominent in dynamically indented regions compared to statically indented regions. Thus these microstructural observations indicated that apart from pre-existing flaws, deformation-induced regions can also act as potential sources for cracking.

While the transgranular microcracks were associated with processing-induced (pre-existing) and deformation-induced (slip-band) flaws, formation of radial microcracks from the ZrB_2–SiC interfaces (see Fig. 5) is associated with mismatch in coefficient of thermal expansion (CTE, α) between the hexagonal ZrB_2 ($\alpha_{avg} \sim 5.9 \times 10^{-6}\,K^{-1}$) phase and the cubic SiC ($\alpha \sim 3.5 \times 10^{-6}\,K^{-1}$) phase.[27] Upon cooling of the consolidated compact from sintering temperature to room temperature, CTE mismatch causes residual tensile radial stress at the ZrB_2–SiC interface in the as-processed composite.[27] These interfaces may also act as potential sources for radial microcraking within the ZrB_2 phase during the indentation process.

The low- and high-velocity scratch studies also revealed similar microcracking features within the ZrB_2 phase (Figs. 8(b) and 9(b)). However, these cracks were perpendicular to the scratch path. The scratches at high-velocity and high-load revealed extensive microcracking compared to those at low-velocity and low-load. Using the combined elastic stress field solutions of Boussinesq and Cerruti provided in Johnson,[28] it has been shown previously[15] that the maximum principal stress (σ_1) is tensile in the wake of the indenter and is oriented parallel to the scratch direction. Thus with increase in scratch load the magnitude of this stress increases and leads to the formation of orthogonal transgranular microcracks.

Apart from microcracking, the high-velocity scratch experiments caused lateral crack evolution and significant material removal in the composite which was almost absent in low-velocity scratches, see Figs. 8(a) and 9(a). It is known from numerous experimental and theoretical investigations that the loading phase of scratch process causes elastic–plastic deformation within a brittle material.[7] Therefore, upon unloading residual stress is generated within the material. It has been well-known that scratch-induced residual stress component perpendicular to the scratch surface causes lateral cracking.[7] In Fig. 2, subsurface lateral crack growth within a constant load scratch groove at 250 mN can be observed. However, due to the low-load level used in these experiments, extension of the lateral crack up to the top surface was limited. During high-velocity scratches, the applied scratch load was significantly higher and resulted in extensive lateral cracking as seen in Fig. 9(a).

One interesting deformation feature evolved during the indentation and the scratch experiments in the composite was the slip-line formation within the ZrB_2 matrix. This feature suggested dislocation activity and was confirmed from preliminary TEM studies (Fig. 10). Although the specific slip-systems activated during indentation and scratch experiments were not identified in the current work, random orientation of the slip-lines along the scratch length was attributed to the random orientation of ZrB_2 grains with respect to the scratch direction. Plasticity in ceramics, in general, is limited due to small number of slip systems and low dislocation mobility.[29] With an increase in load, fracture stress is achieved well before plasticity can initiate and hence the material fails in brittle fashion. However, plasticity can initiate in ceramics under confined conditions such as in indentation and scratch experiments where the material directly beneath the tool experiences large compressive and shear stresses. Once plasticity is initiated, due to low dislocation mobility stress concentration occurs at dislocation pile-ups which can lead to microcracking to relieve the applied stress.[29] Therefore, while the formation of slip-lines is clear evidence of dislocation activity, microcrack formation in these regions is further evidence of stress concentrations associated with limited dislocation mobility, see Fig. 7.

Clearly, the macroscopic manifestation of dislocation activity into slip-lines in the ZrB_2–SiC composite indicates that this composite may have higher fracture toughness compared to the traditional brittle ceramics under static and dynamic loads. Our future research will focus on room temperature and elevated temperature quasistatic and dynamic compression and fracture toughness determination. These studies are expected to provide more insight in to the ductile behavior of the composite.

5. Conclusions

Static indentation, dynamic indentation, and high-velocity scratch investigations revealed several inelastic deformation features such as grain-level transgranular microcracking, lateral cracking and slip-line formation in an ultra-high temperature ZrB_2–SiC composite. Microcracking and slip-line formation were limited to the ZrB_2 phase only.

In indentation studies, the composite exhibited higher dynamic hardness compared to the static hardness. Significant transgranular microcracking within the ZrB_2 matrix was observed in the dynamically indented regions where as such features were absent in static indentations.

In high-velocity scratch experiments, extensive transgranular lateral cracking caused severe brittle damage and material removal in the composite.

Slip-line formation in all the above studies indicated dislocation activity within the ZrB_2 phase. Preliminary TEM studies of the scratch-induced deformation regions confirmed dislocation activity and activation of multiple slip-systems in the ZrB_2 matrix.

Acknowledgement

The electron microscopy equipment used in this study is housed and maintained in the Major Analytical Instrumentation Center at the University of Florida.

References

1. Fahrenholtz, W. G., Hilmas, G. E., Talmy, I. G. and Zaykoski, J. A., Refractory diborides of zirconium and hafnium. *J. Am. Ceram. Soc.*, 2007, **90**, 1347–1364.
2. Rezaie, A., Fahrenholtz, W. G. and Hilmas, G. E., Evolution of structure during the oxidation of zirconium diboride–silicon carbide in air up to 1500 °C. *J. Eur. Ceram. Soc.*, 2007, **27**, 2495–2501.
3. Lawn, B. R. and Evans, A. G., Elastic–plastic indentation damage in ceramics: the median/radial crack system. *J. Am. Ceram. Soc.*, 1980, **63**, 574–581.
4. Cook, R. F. and Pharr, G. M., Direct observation and analysis of indentation cracking in glasses and ceramics. *J. Am. Ceram. Soc.*, 1990, **73**, 787–817.
5. Mukerji, J. and Das, P. K., Wear of some advanced ceramics under a sharp indenter in unidirectional sliding. *J. Am. Ceram. Soc.*, 1993, **76**, 2376–2378.
6. Jahanmir, S., *Friction and Wear of Ceramics*. Mercel Dekker Inc., 1994.
7. Ahn, Y., Farris, T. N. and Chandrasekar, S., Sliding microindentation fracture of brittle materials: role of elastic stress fields. *Mech. Mater.*, 1998, **29**(3), 143–152.
8. Meyers, M. A., *Dynamic Behavior of Materials*. Wiley, New York, 1994.
9. Ravichandran, G. and Subhash, G., A micromechanical model for the high strain rate behavior of ceramics. *Int. J. Solids Struct.*, 1995, **32**, 2627–2646.
10. Chen, W. and Ravichandran, G., Static and dynamic compressive behavior of aluminum nitride under moderate confinement. *J. Am. Ceram. Soc.*, 1996, **79**, 579–584.
11. Sarva, S. and Nemat-Nasser, S., Dynamic compressive strength of silicon carbide under uniaxial compression. *Mater. Sci. Eng. A*, 2001, **A317**, 140–144.
12. Suresh, S., Nakamura, T., Yeshurun, Y., Yang, K. H. and Duffy, J., Tensile fracture toughness of ceramic materials: effects of dynamic loading and elevated temperature. *J. Am. Ceram. Soc.*, 1990, **73**, 2457.
13. Subhash, G., Dynamic indentation testing. *ASM Handbook on Mechanical Testing and Evaluation*, 2000, **8**, pp. 519–529.
14. Subhash, G., Maiti, S., Geubelle, P. H. and Ghosh, D., Recent advances in dynamic indentation fracture, impact damage and fragmentation of ceramics. *J. Am. Ceram. Soc.*, 2008, **91**(9), 2777–2791.
15. Ghosh, D., Subhash, G., Sudarshan, T. S. and Radhakrishanan, R., Scratch-induced microplasticity and microcracking in zirconium diboride-silicon carbide composite. *Acta Mater.*, 2008, **56**, 3011–3022.
16. Subhash, G., Marszalek, M. A. and Maiti, S., Sensitivity of scratch resistance to grinding-induced damage anisotropy in silicon nitride. *J. Am. Ceram. Soc.*, 2006, **89**, 2528–2536.
17. Subhash, G. and Zhang, H., Dynamic indentation response of ZrHf-based bulk metallic glasses. *J. Mater. Res.*, 2007, **22**, 478–485.
18. Giannuzzi, L. A. and Stevie, F. A., *Introduction to Focused Ion Beams: Instrumentation, Theory, Techniques and Practice*. Springer, New York, 2005, pp. 201–212.
19. Haggerty, J. S. and Lee, D. W., Plastic deformation of ZrB_2 single crystals. *J. Am. Ceram. Soc.*, 1971, **54**, 572–576.
20. Shih, C. J., Meyers, M. A., Nesterenko, V. F. and Chen, S. J., Damage evolution in dynamic deformation of silicon carbide. *Acta Mater.*, 2000, **48**, 2399–2420.
21. Forquin, P., Tran, L., Louvigne, P.-F., Rota, L. and Hild, F., Effect of aluminum reinforcement on the dynamic fragmentation of SiC ceramics. *Int. J. Impact Eng.*, 2003, **28**, 1061–1076.
22. Normandia, M. J., Impact response and analysis of several silicon carbides. *Int. J. Appl. Ceram. Technol.*, 2004, **1**, 226–234.
23. Iyer, K. A., Relationships between multiaxial stress states and internal fracture patterns in sphere-impacted silicon carbide. *Int. J. Fract.*, 2007, **146**, 1–18.
24. Subhash, G. and Ravichandran, G., Split-Hopkinson pressure bar testing of ceramics. *ASM Handbook on Mechanical testing and Evaluation*, 2000, **8**, pp. 497–504.
25. Wang, H. and Ramesh, K. T., Dynamic strength and fragmentation of hot-pressed silicon carbide under uniaxial compression. *Acta Mater.*, 2003, **52**, 355–367.
26. Deng, H. and Nemat-Nasser, S., Dynamic damage evolution of solids in compression: microcracking, plastic flow, and brittle–ductile transition. *J. Eng. Mater. Technol.*, 1994, **116**, 286–289.
27. Ghosh, D., Subhash, G. and Orlovskaya, N., Measurement of scratch-induced residual stress within SiC grains in ZrB_2–SiC composite using micro-Raman spectroscopy. *Acta Mater.*, 2008, **56**, 5345–5354.
28. Johnson, K. L., *Contact Mechanics*. Cambridge University Press, Cambridge, 1985.
29. Lankford, J., Predebon, W. W., Staehler, J. M., Subhash, G., Pletka, B. J. and Anderson, C. E., The role of plasticity as limiting factor in the compressive failure of high strength ceramics. *Mech. Mater.*, 1998, **29**, 205–218.